CrossMark

ARTICLE

Self-Decoration of PtNi Alloy Nanoparticles on Multiwalled Carbon Nanotubes for Highly Efficient Methanol Electro-Oxidation

Yu-Yan Zhou[1] · Chang-Hai Liu[2] · Jie Liu[1] · Xin-Lei Cai[1] · Ying Lu[1] · Hui Zhang[1] · Xu-Hui Sun[1] · Sui-Dong Wang[1]

Abstract A simple one-pot method was developed to prepare PtNi alloy nanoparticles, which can be self-decorated on multiwalled carbon nanotubes in [BMIm][BF$_4$] ionic liquid. The nanohybrids are targeting stable nanocatalysts for fuel cell applications. The sizes of the supported PtNi nanoparticles are uniform and as small as 1–2 nm. Pt-to-Ni ratio was controllable by simply selecting a PtNi alloy target. The alloy nanoparticles with Pt-to-Ni ratio of 1:1 show high catalytic activity and stability for methanol electro-oxidation. The performance is much higher compared with those of both Pt-only nanoparticles and commercial Pt/C catalyst. The electronic structure characterization on the PtNi nanoparticles demonstrates that the electrons are transferred from Ni to Pt, which can suppress the CO poisoning effect.

Graphical Abstract
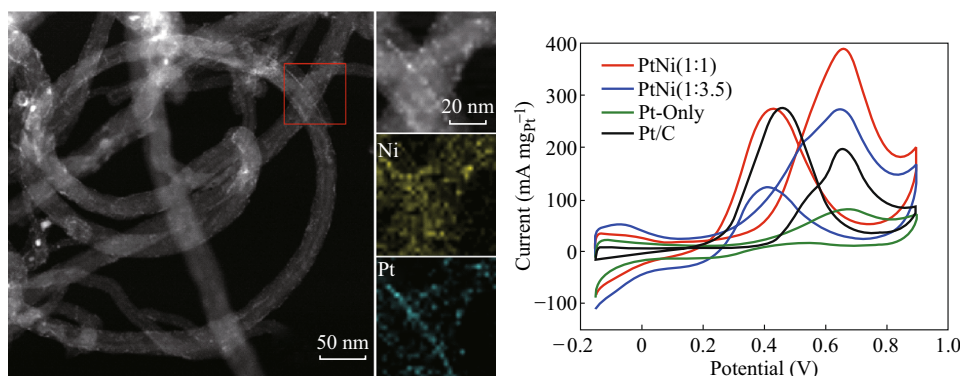
Electronic supplementary material The online version of this article (doi:10.1007/s40820-016-0096-2) contains supplementary material, which is available to authorized users.

✉ Chang-Hai Liu
liuch@cczu.edu.cn

✉ Sui-Dong Wang
wangsd@suda.edu.cn

1 Institute of Functional Nano & Soft Materials (FUNSOM), Jiangsu Key Laboratory for Carbon-Based Functional Materials & Devices, Soochow University, Suzhou 215123, Jiangsu, People's Republic of China

2 School of Materials Science & Engineering, Jiangsu Collaborative Innovation Center of Photovoltaic Science and Engineering, Changzhou University, Changzhou 213164, Jiangsu, People's Republic of China

1 Introduction

To satisfy increasing demands in energy and overcome issues of environment pollution, researches on sustainable and renewable energy which may replace traditional fossil fuels have become hot topics. Direct methanol fuel cells (DMFCs), a green power sources in vehicles and portable devices, have gained wide attentions [1–3]. Methanol as fuel has numerous advantages: simplicity in handling, storage, and transport; low cost and renewability

because it can be easily obtained from fermentation of agricultural products [4–6]. The efficiency of methanol electro-oxidation is limited by poor kinetics and methanol crossover [6, 7], and thus the development of anode catalysts with high catalytic performance is in an urgent need to achieve efficient DMFCs. Pt is the most widely used catalyst for electrochemical oxidation of methanol. However, during the electro-oxidation process, CO molecules are produced as the intermediate, which could be adsorbed on the Pt surface and hardly be removed. As a consequence, the surface poisoning of Pt by CO will suppress the catalytic activity, and this issue must be addressed for the realization of efficient and stable Pt catalysts [7, 8].

The methanol electro-oxidation on Pt is considered to follow a three-step process. The first is the adsorption of methanol. Subsequently, Pt breaks the C–H bonds of methanol and then CO molecules will adsorb on the Pt surface, which is regarded as the dehydrogenation step. Eventually, CO is oxidized with the assistance of oxygen-containing species (e.g., –OH) formed on Pt [9, 10]. However, the oxygen-containing species are often formed on the Pt surface at high potentials [>0.7 V vs reversible hydrogen electrode (RHE)] [7, 10, 11]. Therefore, at the state of low potentials, the adsorbed CO molecules are very difficult to be removed, which results in poor activity of Pt catalysts.

Introducing a second or third metal, such as Ni, Au, Ru, Sn, Co, or Cu [12–19], is an effective way to liberate the Pt surface from the CO adsorption. In this type of bimetallic systems, Pt plays a key role for the adsorption of methanol and dehydrogenation. On the other hand, the second metal could supply oxygen-containing species as the promoter for the CO oxidation at low potentials [20]. The second metal could also modify the electronic structure of Pt by transferring electrons from the second metal to Pt and thus weakening the Pt–CO bonding energy [21, 22]. The binary and ternary Pd-based catalysts were also along the same path [23, 24]. Furthermore, the addition of a second metal will reduce the consumption of Pt, which is in favor of minimizing the catalyst cost.

Among bimetallic catalysts, PtNi nanoparticles (NPs) in particular are promising materials for methanol electro-oxidation since Ni is more economic than other metals [14, 22, 25]. PtNi catalysts with enhanced activity have been prepared by the microwave-assisted polyol reduction, and the enhancement in catalytic activity is attributed to their electronic structure modification [7]. The X-ray photoelectron spectroscopy (XPS) results show that the Pt 4f peak for PtNi is shifted to the lower binding energy, demonstrating the electron transfer from Ni to Pt [7]. The density functional theory (DFT) studies further indicate that incorporating Ni will induce an upshift in the d-band center of Pt, leading to a weakening of the interaction between Pt and CO [14, 26].

The reduction of metal ions in solution is a typical approach to synthesize metal and alloy NPs [25, 27], which often involves chemical additives and/or byproducts, such as surfactants or polymers used to stabilize metal NPs. However, the introduction of the organic materials would block the active surface of metal and alloy NPs to some extent. To realize an additive/byproduct free approach, we develop a room-temperature ionic liquid (RTIL)-assisted sputtering method to prepare supported metal and alloy NPs. RTILs herein play an important role for uniform dispersion of nanosupports and stabilization of small-sized metal NPs. In this method, metal is directly sputtered onto a suspension mixing RTILs and nanosupports [28–31], where metal NPs may nucleate on the RTIL surface, and then diffuse into the suspension and finally self-decorate on the nanosupports [24, 32–34]. This method has been extended to prepare supported bimetallic NPs, such as AgPd and AgAu NPs decorated on graphene, and PdAu NPs decorated on carbon or TiO_2 nanosupports [31, 35–37].

The RTIL-assisted sputtering is utilized to synthesize PtNi alloy NPs decorated on multiwalled carbon nanotubes (MWNTs), which possess large surface area, high conductivity, and good chemical stability. In particular, the PtNi NPs were prepared straightforwardly by sputtering a PtNi alloy target, and thus the atomic ratio of Pt to Ni can be easily controlled by changing the alloy target. The self-decoration on MWNTs is demonstrated to be an effective way to stabilize the PtNi alloy NPs, which have small sizes of only a few nanometers and uniform distribution on the nanosupport. Upon the employment of an appropriate Pt-to-Ni ratio, the supported PtNi NPs showed high catalytic activity and high stability for methanol electro-oxidation. The catalytic performance of the alloy NPs is superior to those of the Pt-only NPs and the commercial Pt/C catalyst.

2 Experimental

2.1 Preparation of Pt/PtNi-NP-MWNT Hybrids

RTIL, 1-butyl-3-methylimidazolium tetrafluoroborate ([BMIm][BF$_4$]), purity >99 %), was purchased from Shanghai Cheng-Jie Chemical and dried in vacuum for 24 h before using. MWNTs with diameters ranging from 30 to 50 nm were purchased from Nanjing XFNANO Materials Tech. The commercial Pt/C catalyst was purchased from Alfa Aesar.

Firstly, 10 mg MWNTs was fully dispersed into 1.5 mL [BMIm][BF$_4$], with ultrasonication for 30 min to produce the [BMIm][BF$_4$]-MWNT suspension. A stainless steel pot containing the suspension was placed into the sputtering chamber. A Pt or PtNi alloy target was used to sputter Pt or

PtNi, respectively, onto the suspension for 15 min in a desktop direct-current sputtering system (Quorum Technologies). Two PtNi alloy targets were selected: one is Pt rich and the other is relatively Ni rich. The actual Pt-to-Ni ratio of the PtNi NPs was estimated by inductively coupled plasma atomic emission spectroscopy (ICP-AES, Vista-MPX), and two Pt-to-Ni atomic ratios of 1:1 and 1:3.5 were obtained. During the sputtering, the Ar working pressure and deposition rate were kept at ~ 0.01 mbar and 0.2 Å s^{-1}, respectively. Eventually, the Pt/PtNi-NP-MWNT hybrids were separated from [BMIm][BF$_4$] by centrifugation, and the supernatant liquid was decanted after the centrifugation. The hybrids were then washed by acetone several times to completely remove residual [BMIm][BF$_4$]. To liberate the catalysts from possible surface contamination, the hybrids were annealed at ~ 300 °C for 1 h in H$_2$-Ar environment (~ 2.5 mbar, H$_2$:Ar = 1:9).

2.2 Characterization of Pt/PtNi-NP-MWNT Hybrids

The metal loading and composition of the hybrids were analyzed by ICP-AES, and the measured Pt loading is shown in Table 1. The Pt-based catalysts were sampled by treating with aqua regia. MWNTs cannot be dissolved, and then were discarded by centrifugation. Pt and Ni were dissolved and left in solution for the ICP-AES measurements. To confirm the validity of the ICP-AES results, a commercial Pt/C catalyst with known metal loading of 20 wt% was also measured as reference. The microscopic structures of the hybrids were characterized with high-resolution transmission electron microscopy (HRTEM, FEI Quanta FRG 200F) and high-angle annular dark-field scanning TEM (HAADF-STEM). The electronic structures of the hybrids were characterized with XPS (Kratos Axis Ultra DLD, monochromatic Al $K\alpha$ source). The X-ray absorption near-edge structure (XANES) measurements of the hybrids were performed at the Taiwan light source (TLS).

2.3 Electrochemical Measurements

The electrochemical measurements were carried out using CHI660E with three-electrode configuration. A carbon electrode was used as the counter electrode, and an Ag/AgCl electrode was used as the reference electrode with respect to which potentials were measured. On the other hand, a catalyst-coated glassy carbon (GC) electrode (3 mm in diameter) was employed as the working electrode. Before the preparation of the working electrode, the GC electrode was polished using an alumina slurry of 0.05 μm. Subsequently, the GC electrode was ultrasonically washed in a mixed solution of ethanol and deionized water of 1:1 in volume, and then dried at room temperature.

The catalyst suspensions were obtained by fully dispersing 3 mg catalyst in a mixed solution of 1 mL ethanol and 7 μL Nafion solution (5 wt% purchased from Aldrich) with ultrasonication for 1 h. The working electrode was prepared by dropping 10 μL catalyst ink onto the GC electrode and then drying it in air, yielding a working electrode with a catalyst loading of 0.42 mg cm^{-2}. The actual mass of Pt in the catalyst ink were 5.96, 1.75, 1.39, and 0.85 μg for Pt/C, Pt-only, PtNi (1:1) and PtNi (1:3.5), respectively. Cyclic voltammogram (CV) was carried out with typical parameters, at a scan rate of 50 mV s^{-1} in a solution of 1 M CH$_3$OH + 0.5 M H$_2$SO$_4$, to evaluate the catalytic activity for methanol electro-oxidation.

3 Results and Discussion

3.1 Microscopic Structures

The metal composition and loading of the as-prepared nanocatalysts and commercial Pt/C catalyst were measured by ICP-AES, and the results are summarized in Table 1. The sputtering of a Pt-rich alloy target produces the PtNi NPs with measured Pt-to-Ni ratio of about 1:1. Ni appears to be easier to decorate onto MWNTs in [BMIm][BF$_4$] compared with Pt [38, 39], presumably due to the fact that Ni is more active than Pt. On the other hand, employing a relatively Ni-rich alloy target leads to the PtNi NPs with measured Pt-to-Ni ratio of about 1:3.5. The two groups of PtNi samples with different Pt-to-Ni ratios and the pure Pt hybrid as the control sample were denoted as the PtNi (1:1), PtNi (1:3.5), and Pt-only NPs, respectively.

Figure 1a, d, g shows the TEM images of the Pt/PtNi-NP-MWNT hybrids, which exhibit uniform size distribution and good dispersion of NPs on MWNTs. The average NP diameters are 1.34, 1.73, and 1.83 nm for the Pt-only, PtNi (1:1), and PtNi (1:3.5) NPs, respectively. Upon addition of Ni, the NP size is only slightly increased, and it is much smaller than that in the commercial Pt/C catalyst (average Pt NP diameter of 4.04 nm, see Fig. S1 in Supporting Information). Figure 1b, e, h shows the typical HRTEM images of the Pt-only, PtNi (1:1), and PtNi (1:3.5) NPs, respectively. The interplanar spacing of 0.226 nm for

Table 1 Metal composition of different catalysts measured by ICP-AES

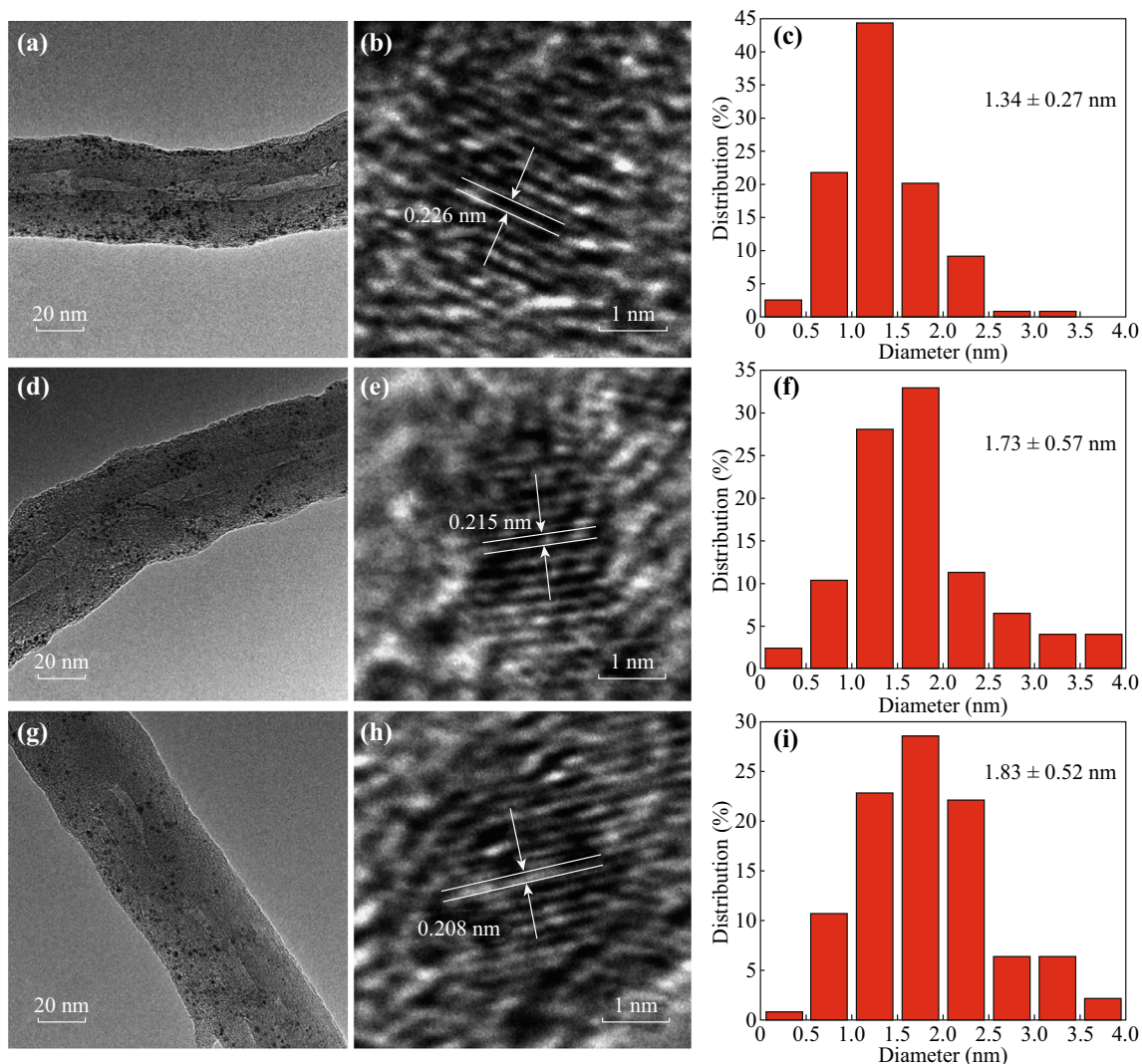| Catalyst	Metal loading [wt%]		Atomic ratio of Pt:Ni
	Pt	Ni	
Pt/C	19.22	–	–
Pt-only	7.74	–	–
PtNi (1:1)	6.76	1.91	1:1
PtNi (1:3.5)	3.35	3.48	1:3.5

Fig. 1 TEM images, HRTEM images, and NP size distributions in Pt/PtNi-NP-MWNT hybrids: **a–c** Pt-only NPs; **d–f** PtNi (1:1) NPs; and **g–i** PtNi (1:3.5) NPs

Pt-only matches well with the (111) plane of face-centered-cubic (fcc) Pt [40]. Upon introduction of Ni, the spacing value is gradually decreased, e.g., the PtNi (1:1) NPs exhibit the interplanar spacing of 0.217 nm and the PtNi (1:3.5) NPs show the one of 0.208 nm. The lattice contraction suggests that the PtNi NPs are in an alloy form [41].

The HAADF-STEM technique was utilized to verify the spatial distribution of Pt and Ni in the PtNi-NP-MWNT hybrids, and the results are shown in Fig. 2. The dark-field images show that the PtNi NPs are decorated on the entire surface of MWNTs. The STEM mapping demonstrates the uniformity and overlapping in spatial distribution for both Pt and Ni, supporting the alloying of the PtNi NPs regardless of Pt-to-Ni ratio. The microscopic structure results indicate that the PtNi NPs can self-decorate onto

MWNTs in [BMIm][BF$_4$] and maintain the small NP size and uniform NP distribution.

3.2 Electronic Structures

XPS was used to analyze the chemical states of the Pt/PtNi-NP-MWNT hybrids, and the XPS Pt 4f spectra are shown in Fig. 3a, where a vertical reference line is present. Compared with the Pt 4$f_{7/2}$ peak of bulk Pt at binding energy of about 71 eV, there is a significant shift of the Pt 4$f_{7/2}$ peak to higher binding energy for the hybrids. The increase in binding energy may be due to the small NP size and the interaction of Pt with the support [42, 43]. Upon the addition of Ni, the Pt 4$f_{7/2}$ peak of the PtNi (1:1) NPs is negatively shifted compared to that of the Pt-only NPs. With increasing the proportion of Ni, the Pt 4$f_{7/2}$ peak of
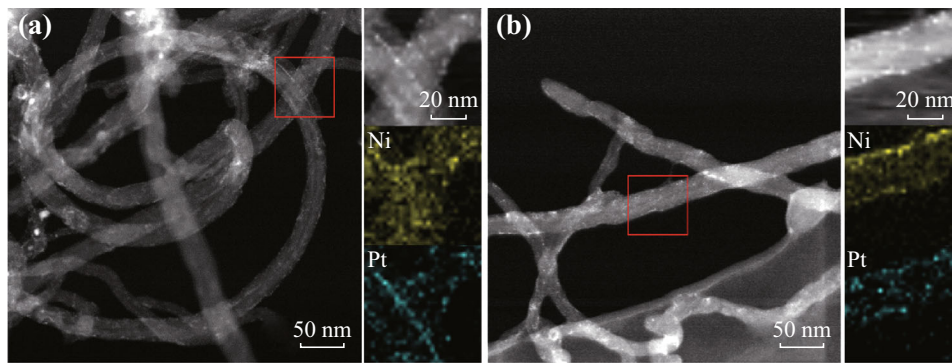
Fig. 2 HAADF-STEM images of **a** PtNi (1:1) NPs and **b** PtNi (1:3.5) NPs on MWNTs, where elemental mapping of Pt and Ni is shown
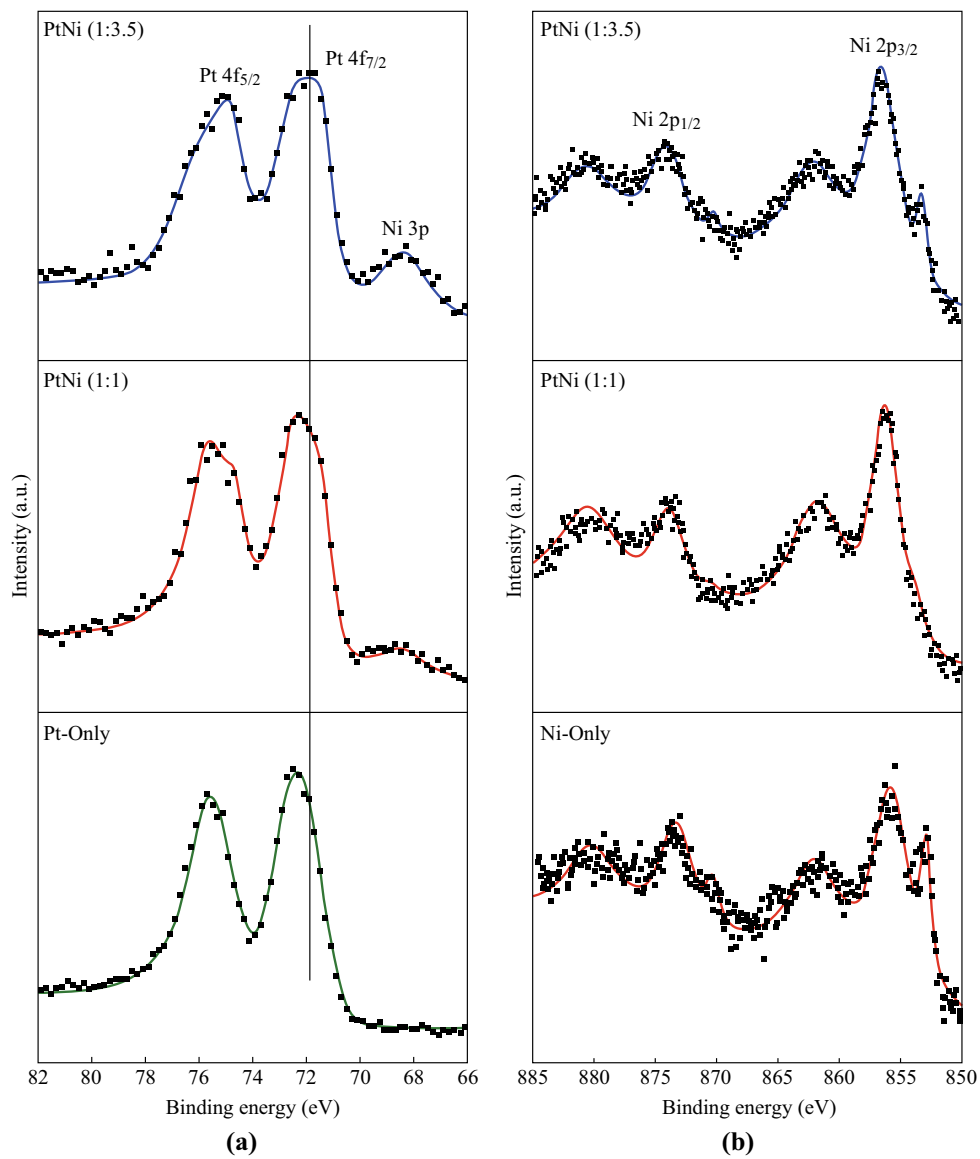

Fig. 3 XPS spectra of Pt/Ni/PtNi-NP-MWNT hybrids: **a** Pt 4*f* region and **b** Ni 2*p* region

376

Nano-Micro Lett. (2016) 8(4):371–380

the PtNi (1:3.5) is further shifted to lower binding energy. Such shifts in binding energy suggest the electron transfer from Ni to Pt arising from the PtNi alloy formation [40].

On the other hand, the XPS Ni $2p$ spectra of the hybrids are shown in Fig. 3b for comparison. In all the spectra, the Ni oxidized state (e.g., at binding energy of about 856 eV) together with a broad satellite peak at higher binding energy account for the vast majority. The Ni metallic state at binding energy of about 853 eV is present as well, whereas it is gradually disappeared with increasing the Pt proportion. The XPS Ni features are consistent with the Pt ones, indicating an electron loss of Ni and an electron gaining of Pt in the PtNi NPs.

To make a double check on the electronic structures of the PtNi NPs, the Pt L_3-edge XANES spectra were measured at the TLS and the results are shown in Fig. 4. The absorption peak at about 11.57 keV corresponds to the electronic transition from Pt $2p$ to $5d$, and the absorption edge called as the whiteline can reflect the density of unoccupied states in the d-band of Pt. The whiteline intensity decreases with decrease of unoccupied states in $5d$ band [7]. As demonstrated in Fig. 4, the whiteline intensity for the Pt/PtNi-NP-MWNT hybrids is lower than that for Pt/C. Furthermore, the whiteline intensity for the PtNi NPs is lower compared with the Pt-only NPs, in particular upon increasing the proportion of Ni. The XANES results imply that the PtNi NPs possess less unoccupied states in the d-band of Pt due to the electron transfer from Ni to Pt, in good agreement with our argument of the PtNi alloy formation.

3.3 Electrochemical Performance

The electrochemical performance of the Pt/PtNi-NP-MWNT hybrids was characterized by the CV curves as shown in Fig. 5. The CV curves are featured with three
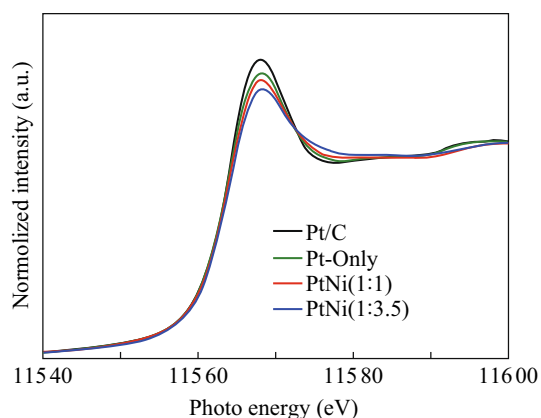

Fig. 4 Pt L_3-edge XANES spectra of Pt/PtNi-NP-MWNT hybrids and commercial Pt/C catalyst

parts: the hydrogen region, the double-layer region, and Pt oxidation–reduction region. Due to a more negative oxidation potential of Ni, no characteristic features of Ni oxidation–reduction are observed in the scan range [44]. The electrochemical surface area (ECSA) was calculated based on the desorption area of hydrogen (dash area in CV) [41, 45]. The ECSA values for the Pt/C, Pt-only, PtNi (1:1), and PtNi (1:3.5) catalysts are 18.71, 15.57, 36.65, and 28.98 m^2 (g$_{Pt}$)$^{-1}$, respectively. Thus, the alloying of Pt and Ni is in favor of increasing ECSA, and Pt-to-Ni ratio turns out to be critical to the electrochemical performance.

To evaluate the catalytic activity of the hybrids for methanol electro-oxidation, as depicted in Fig. 6a, the stable CV data were recorded in a N$_2$-purged CH$_3$-OH + H$_2$SO$_4$ solution at a scan rate of 50 mV s^{-1}. In the CV curves, two characteristic peaks are present in forward and backward scans, respectively. The ratio of the Pt-mass-normalized peak current in forward scan (I_f) and that in backward scan (I_b) is considered as a hint of the catalytic resistance to the CO poisoning, and a higher I_f/I_b ratio may correspond to stronger CO poisoning tolerance [46–48]. The I_f/I_b ratios of the Pt/PtNi-NP-MWNT hybrids are significantly higher than that of the commercial Pt/C catalyst, as summarized in Table 2. The Pt-only NPs have a maximum I_f/I_b ratio; however, in this case the I_f value is very small presumably due to limited Pt active sites arising from surface oxidation. The surface oxidation of the Pt-only NPs will suppress the adsorption of methanol molecules and accordingly the CO poisoning as well.

On the other hand, the onset potential for methanol electro-oxidation is another important parameter to evaluate the catalytic performance [49]. In forward scan, the onset potentials are 0.38, 0.32, and 0.29 V for the Pt-only, PtNi (1:1), and PtNi (1:3.5) NPs, respectively, all of which are lower than the one of 0.40 V for the commercial Pt/C catalyst. Significantly, the addition of Ni can effectively lower the onset potential, indicating the superiority of the PtNi alloy NPs for methanol electro-oxidation. As shown in Table 2, the PtNi (1:1) and PtNi (1:3.5) NPs show much larger I_f of 390 and 274 mA (mg$_{Pt}$)$^{-1}$, respectively, in comparison to that of Pt/C (198 mA (mg$_{Pt}$)$^{-1}$). The trend in I_f is well consistent with the ECSA results shown in Fig. 5.

According to the XPS and XANES results, the electronic structure of Pt was modified by the electron transfer from Ni, which will reduce the density of unoccupied states in the Pt d-band and hence weaken the Pt–CO bonding. In addition, the oxygen-containing species, which may be produced from Ni(OH)$_2$, can react with adsorbed CO on the Pt surface [50]. This process will promote CO oxidation and then liberate the Pt surface from CO adsorption. Therefore, the PtNi alloy NPs show much higher catalytic activity than the Pt monometallic counterpart. However,
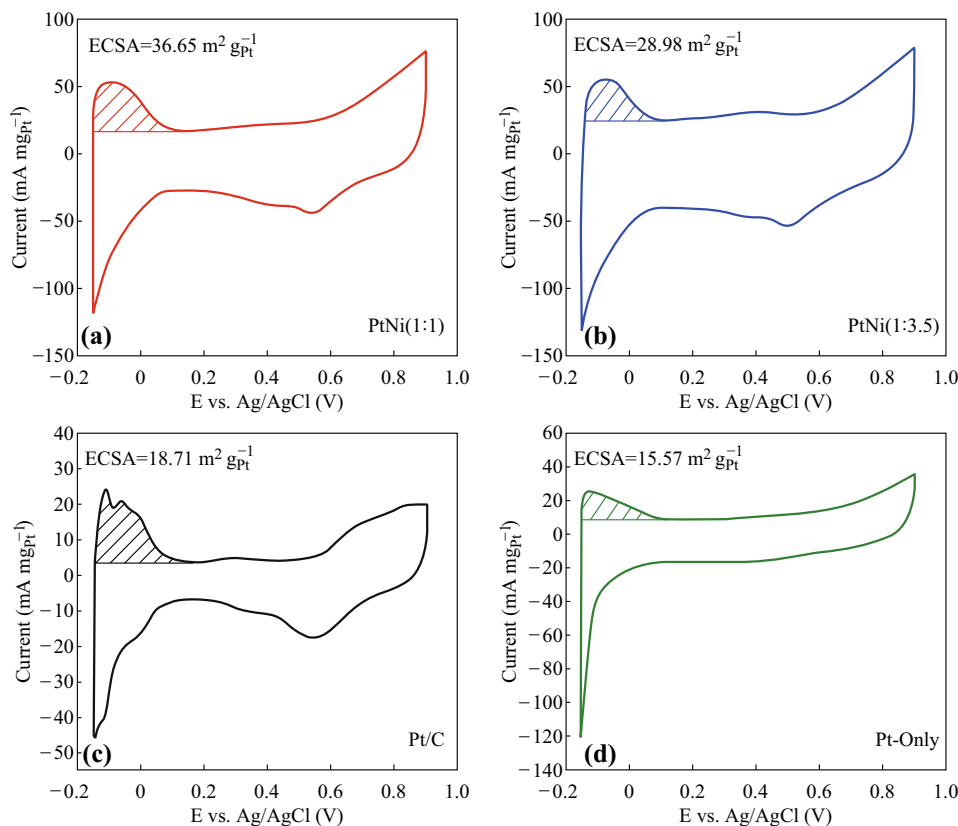
Fig. 5 Cyclic voltammetry curves of **a** PtNi (1:1) NPs, **b** PtNi (1:3.5) NPs, **c** commercial Pt/C catalyst, and **d** Pt-only NPs, measured at room temperature in 0.5 M H_2SO_4 with a scan rate of 50 mV s^{-1}
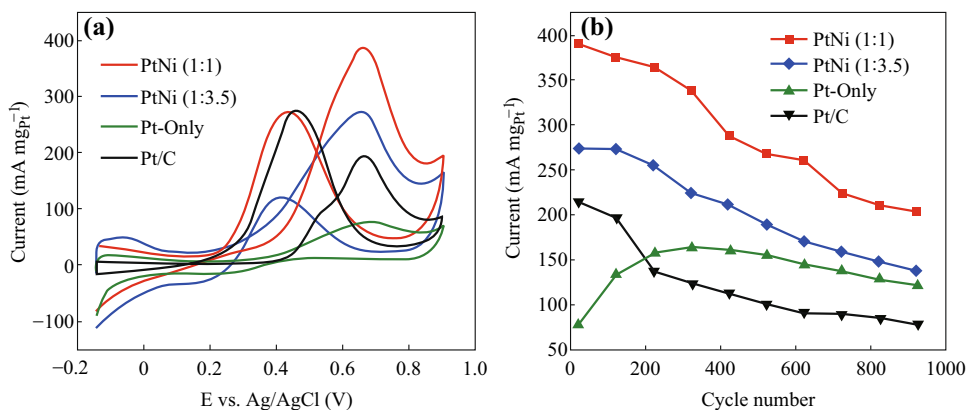

Fig. 6 **a** Cyclic voltammetry curves of Pt/PtNi-NP-MWNT hybrids and commercial Pt/C catalyst, and **b** Pt-mass-normalized peak current versus cycle number, measured at room temperature in 1 M CH_3OH + 0.5 M H_2SO_4 with a scan rate of 50 mV s^{-1}

excess Ni would cover the surface of Pt active sites and thus decrease the catalytic activity, such as in the case of the PtNi (1:3.5) NPs compared with the PtNi (1:1) NPs. As a consequence, an appropriate Pt-to-Ni ratio is needed to reach the highest catalytic performance. For instance, the PtNi (1:1) NPs are considered as having sufficient active sites and strong resistance against the CO poisoning at the same time.

Figure 6b shows a comparison in I_f of the studied catalysts in multiple CV cycles. After over 900 CV cycles, I_f of the PtNi (1:1) and PtNi (1:3.5) NPs maintain 52.1 and 50.5 % of their initial ones, respectively. In contrast, I_f of the commercial Pt/C catalyst maintains only 36.6 % of its initial one. The results demonstrate the long-term stability of the PtNi-NP-MWNT hybrids. As for the Pt-only NPs, I_f is increased first and then decreased with raising the cycle

378

Nano-Micro Lett. (2016) 8(4):371–380

Table 2 Electrochemical parameters of different catalysts calculated from cyclic voltammetry curve

Catalyst	Pt/C	Pt-only	PtNi (1:1)	PtNi (1:3.5)
ECSA $[m^2\ (g_{Pt})^{-1}]$	18.71	15.57	36.65	28.98
Onset potential [V]	0.40	0.38	0.32	0.29
I_f [mA $(mg_{Pt})^{-1}$]	198	80	390	274
I_b [mA $(mg_{Pt})^{-1}$]	277	15	273	122
I_f/I_b	0.7	5.3	1.4	2.2

number. The origin of the I_f increase in the beginning is unclear so far, whereas it is worth noting that I_f for the Pt-only NPs are always smaller than those for the PtNi alloy NPs in all the cycles.

4 Conclusion

The PtNi alloy NPs decorated on MWNTs were successfully prepared by the RTIL-assisted sputtering method with a PtNi alloy target. The PtNi alloy NPs exhibit small size and uniform distribution, and significantly Pt-to-Ni ratio can be controlled by selecting an appropriate alloy target. The PtNi-NP-MWNT hybrids are demonstrated to have high catalytic activity and long-term stability for methanol electro-oxidation, which are far superior to both the Pt-only monometallic counterpart and the commercial Pt/C catalyst. The XPS and XANES results indicate the electron transfer from Ni to Pt in the PtNi NPs, and it is beneficial to reducing the CO poisoning on the Pt surface. The present approach is promising for simple preparation of alloy-based nanocatalysts used in high-performance DMFCs.

References

1. R. Dillon, S. Srinivasana, A.S. Aricò, V. Antonucci, International activities in DMFC R&D: status of technologies and potential applications. J. Power Sources 127(1), 112–126 (2004). doi:10.1016/j.jpowsour.2003.09.032
2. S.K. Kamarudin, F. Achmad, W.R.W. Daud, Overview on the application of direct methanol fuel cell (DMFC) for portable electronic devices. Int. J. Hydrog. Energy 34(12), 6902–6916 (2009). doi:10.1016/j.ijhydene.2009.06.013
3. J.S. Liang, K.Y. Liu, S.Z. Li, D.Z. Wang, T.Q. Ren, X.Y. Xu, Y. Luo, Novel flow field with superhydrophobic gas channels prepared by one-step solvent-induced crystallization for micro direct methanol fuel cell. Nano-Micro Lett. 7(2), 165–171 (2015). doi:10.1007/s40820-015-0032-x
4. G.W. Huber, S. Iborra, A. Corma, Synthesis of transportation fuels from biomass: chemistry, catalysts, and engineering. Chem. Rev. 106(9), 4044–4098 (2006). doi:10.1021/cr068360d
5. C.N. Hamelinck, A.P.C. Faaij, Outlook for advanced biofuels. Energy Policy 34(17), 3268–3283 (2006). doi:10.1016/j.enpol.2005.06.012
6. E.L. Gyenge, J. Zhang, PEM fuel cell electrocatalysts and catalyst layers: fundamentals and applications. Platin. Met. Rev. 53(4), 219–220 (2009). doi:10.1007/978-1-84800-936-3
7. A.B.A.A. Nassr, I. Sinev, M.M. Pohl, W. Grünert, M. Bron, Rapid microwave-assisted polyol reduction for the preparation of highly active PtNi/CNT electrocatalysts for methanol oxidation. ACS Catal. 4(4), 2449–2462 (2014). doi:10.1021/cs401140g
8. A. Hamnett, Mechanism and electrocatalysis in the direct methanol fuel cell. Catal. Today 38(4), 445–457 (1997). doi:10.1016/S0920-5861(97)00054-0
9. X. Zhao, M. Yin, L. Ma, L. Liang, C. Liu, J. Liao, T. Lu, W. Xing, Recent advances in catalysts for direct methanol fuel cells. Energy. Environ. Sci. 4(4), 2736–2753 (2011). doi:10.1039/c1ee01307f
10. J. Zhang, H. Liu, Electrocatalysis of Direct Methanol Fuel Cells: from Fundamentals to Applications (Wiley, Weinheim, 2009), pp. 227–255
11. S. Wasmus, A. Küver, Methanol oxidation and direct methanol fuel cells: a selective review. J. Electroanal. Chem. 461, 14–31 (1999). doi:10.1016/S0022-0728(98)00197-1
12. J.H. Choi, K.W. Park, I.S. Park, K. Kim, J.S. Lee, Y.E. Sung, A PtAu nanoparticle electrocatalyst for methanol electro-oxidation in direct methanol fuel cells. J. Electrochem. Soc. 153(10), A1812–A1817 (2006). doi:10.1149/1.2224055
13. H.X. Zhao, Z. Zheng, J. Li, H.M. Jia, K.W. Wong, Y.D. Zhang, W.M. Lau, Substitute of expensive Pt with improved electrocatalytic performance and higher resistance to CO poisoning for methanol oxidation: the case of synergistic Pt-Co₃O₄ nanocomposite. Nano-Micro Lett. 5(4), 296–302 (2013). doi:10.1007/BF03353761
14. C.X. Xu, J.G. Hou, X.H. Pang, X.J. Li, M.L. Zhu, B.Y. Tang, Nanoporous PtCo and PtNi alloy ribbons for methanol electrooxidation. Int. J. Hydrog. Energy 37(14), 10489–10498 (2012). doi:10.1016/j.ijhydene.2012.04.041
15. K. Wang, H.A. Gasteiger, N.M. Markovic, P.N. Ross, On the reaction pathway for methanol and carbon monoxide electrooxidation on Pt-Sn alloy versus Pt-Ru alloy surfaces. J. Electrochim. Acta 41(16), 2587–2593 (1996). doi:10.1016/0013-4686(96)00079-5
16. S. Harish, S. Baranton, C. Coutanceau, J. Joseph, Microwave assisted polyol method for the preparation of Pt/C, Ru/C and PtRu/C nanoparticles and its application in electrooxidation of methanol. J. Power Sources 214, 33–39 (2012). doi:10.1016/j.jpowsour.2012.04.045
17. W.J. Kang, R. Li, D.H. Wei, S.L. Xu, S.Y. Wei, H.B. Li, CTAB-reduced synthesis of urchin-like Pt–Cu alloy nanostructures and catalysis study towards the methanol oxidation reaction. RSC Adv. 2015(5), 94210–94215 (2015). doi:10.1039/C5RA20464J

18. X.G. Wang, F.C. Zhu, Y.W. He, M. Wang, Z.H. Zhang, Z.Z. Ma, R.X. Li, Highly active carbon supported ternary PdSnPtx (x = 0.1–0.7) catalysts for ethanol electro-oxidation in alkaline and acid media. J. Colloid. Interface Sci. **468**, 200–210 (2016). doi:10.1016/j.jcis.2016.01.068

19. M. Wang, Y.W. He, R.X. Li, Z.Z. Ma, Z.H. Zhang, X.G. Wang, Electrochemical activated PtAuCu alloy nanoparticle catalysts for formic acid, methanol and ethanol electro-oxidation. Electrochim. Acta **178**, 259–269 (2015). doi:10.1016/j.electacta.2015.07.157

20. M. Watanabe, S. Motoo, Electrocatalysis by ad-atoms: part III. Enhancement of the oxidation of carbon monoxide on platinum by ruthenium ad-atoms. J. Electroanal. Chem. **60**(3), 275–283 (1975). doi:10.1016/S0022-0728(75)80262-2

21. H. Igarashi, T. Fujino, Y. Zhu, H. Uchida, M. Watanabe, CO tolerance of Pt alloy electrocatalysts for polymer electrolyte fuel cells and the detoxification mechanism. Phys. Chem. Chem. Phys. **3**(3), 306–314 (2001). doi:10.1039/b007768m

22. X.W. Zhou, R.H. Zhang, Z.Y. Zhou, S.G. Sun, Preparation of PtNi hollow nanospheres for the electrocatalytic oxidation of methanol. J. Power Sources **196**(14), 5844–5848 (2011). doi:10.1016/j.jpowsour.2011.02.088

23. F.C. Zhu, G.S. Ma, Z.C. Bai, R.Q. Hang, B. Tang, Z.H. Zhang, X.G. Wang, High activity of carbon nanotubes supported binary and ternary Pd-based catalysts for methanol, ethanol and formic acid electro-oxidation. J. Power Sources **242**(22), 610–620 (2013). doi:10.1016/j.jpowsour.2013.05.145

24. F.C. Zhu, M. Wang, Y.W. He, G.S. Ma, Z.H. Zhang, X.G. Wang, A comparative study of elemental additives (Ni, Co and Ag) on electrocatalytic activity improvement of PdSn-based catalysts for ethanol and formic acid electro-oxidation. Electrochim. Acta **148**(2), 291–301 (2014). doi:10.1016/j.electacta.2014.10.062

25. R.P. Xiu, F.F. Zhang, Z.H. Wang, M. Yang, J.F. Xia, R.J. Gui, Electrodeposition of PtNi bimetallic nanoparticles on three-dimensional graphene for highly efficient methanol oxidation. RSC Adv. **5**(105), 86578–86583 (2015). doi:10.1039/C5RA13728D

26. Q. Jiang, L. Jiang, H. Hou, J. Qi, S. Wang, G. Sun, Promoting effect of Ni in PtNi bimetallic electrocatalysts for the methanol oxidation reaction in alkaline media: experimental and density functional theory studies. J. Phys. Chem. C **114**(46), 19714–19722 (2010). doi:10.1021/jp1039755

27. A.B.A.A. Nassr, I. Sinev, W. Grünert, M. Bron, PtNi supported on oxygen functionalized carbon nanotubes: in depth structural characterization and activity for methanol electrooxidation. Appl. Catal. B **142–143**, 849–860 (2013). doi:10.1016/j.apcatb.2013.06.013

28. C.H. Liu, B.H. Mao, J. Gao, S. Zhang, X. Gao, Z. Liu, S.T. Lee, X.H. Sun, S.D. Wang, Size-controllable self-assembly of metal nanoparticles on carbon nanostructures in room-temperature ionic liquids by simple sputtering deposition. Carbon **50**(8), 3008–3014 (2012). doi:10.1016/j.carbon.2012.02.086

29. T. Torimoto, K. Okazaki, T. Kiyama, K. Hirahara, N. Tanaka, S. Kuwabata, Sputter deposition onto ionic liquids: simple and clean synthesis of highly dispersed ultrafine metal nanoparticles. Appl. Phys. Lett. **89**(24), 243117 (2006). doi:10.1063/1.2404975

30. T. Torimoto, T. Tsuda, K. Okazaki, S. Kuwabata, New frontiers in materials science opened by ionic liquids. Adv. Mater. **22**(11), 1196–1221 (2010). doi:10.1002/adma.200902184

31. C.H. Liu, X.Q. Chen, Y.F. Hu, T.K. Sham, S.D. Wang, One-pot environmentally friendly approach toward highly catalytically active bimetal-nanoparticle-graphene hybrids. ACS Appl. Mater. Interfaces **5**(11), 5072–5079 (2013). doi:10.1021/am4008853

32. H. Wender, L.F. de Oliveira, P. Migowski, A.F. Feil, E. Lissner, M.H.G. Prechtl, S.R. Teixeira, J. Dupont, Ionic liquid surface composition controls the size of gold nanoparticles prepared by sputtering deposition. J. Phys. Chem. C **114**(27), 11764–11768 (2010). doi:10.1021/jp102231x

33. H. Zhang, H. Cui, Synthesis and characterization of functionalized ionic liquid-stabilized metal (gold and platinum) nanoparticles and metal nanoparticle/carbon nanotube hybrids. Langmuir **25**(5), 2604–2614 (2009). doi:10.1021/la803347h

34. W.J. Hong, H. Bai, Y.X. Xu, Z.Y. Yao, Z.Z. Gu, G.Q. Shi, Preparation of gold nanoparticle/graphene composites with controlled weight contents and their application in biosensors. J. Phys. Chem. C **114**(4), 1822–1826 (2010). doi:10.1021/jp9101724

35. C.H. Liu, J. Liu, Y.Y. Zhou, X.L. Cai, Y. Lu, X. Gao, S.D. Wang, Small and uniform Pd monometallic/bimetallic nanoparticles decorated on multi-walled carbon nanotubes for efficient reduction of 4-nitrophenol. Carbon **94**, 295–300 (2015). doi:10.1016/j.carbon.2015.07.003

36. C.H. Liu, R.H. Liu, Q.J. Sun, J.B. Chang, X. Gao, Y. Liu, S.T. Lee, Z.H. Kang, S.D. Wang, Controlled synthesis and synergistic effects of graphene-supported PdAu bimetallic nanoparticles with tunable catalytic properties. Nanoscale **7**(14), 6356–6362 (2015). doi:10.1039/C4NR06855F

37. J.B. Chang, C.H. Liu, J. Liu, Y.Y. Zhou, X. Gao, S.D. Wang, Green-chemistry compatible approach to TiO2-supported PdAu bimetallic nanoparticles for solvent-free 1-phenylethanol oxidation under mild conditions. Nano-Micro Lett. **7**(3), 307–315 (2015). doi:10.1007/s40820-015-0044-6

38. N.C. Cheng, M.N. Banis, J. Liu, A. Riese, X. Li, R.Y. Li, S.Y. Ye, S. Knights, X.L. Sun, Extremely stable platinum nanoparticles encapsulated in a zirconia nanocage by area-selective atomic layer deposition for the oxygen reduction reaction. Adv. Mater. **27**(2), 277–281 (2015). doi:10.1002/adma.201404314

39. N.C. Cheng, M.N. Banis, J. Liu, A. Riese, S.C. Mu, R.Y. Li, T.K. Sham, X.L. Sun, Atomic scale enhancement of metal–support interactions between Pt and ZrC for highly stable electrocatalysts. Energy. Environ. Sci. **8**, 1450–1455 (2015). doi:10.1039/C4EE04086D

40. L.L. Wang, D.F. Zhang, L. Guo, Phase-segregated Pt–Ni chain-like nanohybrids with high electrocatalytic activity towards methanol oxidation reaction. Nanoscale **6**(9), 4635–4641 (2014). doi:10.1039/c4nr00139g

41. Y. Shen, K.J. Xiao, J.Y. Xi, X.P. Qiu, Comparison study of few-layered graphene supported platinum and platinum alloys for methanol and ethanol electro-oxidation. J. Power Sources **278**(278), 235–244 (2015). doi:10.1016/j.jpowsour.2014.12.062

42. Y. Shen, Z.H. Zhang, R.R. Long, K.J. Xiao, J.Y. Xi, Synthesis of ultrafine Pt nanoparticles stabilized by pristine graphene nanosheets for electro-oxidation of methanol. ACS Appl. Mater. Interfaces **6**(17), 15162–15170 (2014). doi:10.1021/am503309h

43. M.G. Manson, Electronic structure of supported small metal clusters. Phys. Rev. B **27**(2), 748–762 (1983). doi:10.1103/PhysRevB.27.748

44. P. Mani, R. Srivastava, P. Strasser, Dealloyed binary PtM3 (M = Cu, Co, Ni) and ternary PtNi3 M (M = Cu, Co, Fe, Cr) electrocatalysts for the oxygen reduction reaction: performance in polymer electrolyte membrane fuel cells. J. Power Sources **196**(2), 666–673 (2011). doi:10.1016/j.jpowsour.2010.07.047

45. D.F.V.D. Vliet, C. Wang, D.G. Li, A.P. Paulikas, J. Greeley et al., Unique electrochemical adsorption properties of Pt-skin surfaces. Angew. Chem. Int. Ed. **124**(13), 3193–3196 (2012). doi:10.1002/ange.201107668

46. R. Mancharan, J.B. Goodenough, Methanol oxidation in acid on ordered NiTi. J. Mater. Chem. **2**(8), 875–887 (1992). doi:10.1039/jm9920200875

47. S. Sharma, A. Ganguly, P. Papakonstantinou, X. Miao, M. Li, J.L. Hutchison, M. Delichatsios, S. Ukleja, Rapid microwave synthesis of CO tolerant reduced graphene oxide-supported platinum electrocatalysts for oxidation of methanol. J. Phys. Chem. C **114**(45), 19459–19466 (2010). doi:10.1021/jp107872z

48. A.M. Hofstead-Duffy, D.J. Chen, S.G. Sun, Y.Y.J. Tong, Origin of the current peak of negative scan in the cyclic voltammetry of methanol electro-oxidation on Pt-based electrocatalysts: a revisit to the current ratio criterion. J. Mater. Chem. **22**(11), 5205–5208 (2012). doi:10.1039/c2jm15426a

49. L.X. Ding, A.L. Wang, G.R. Li, Z.Q. Liu, W.X. Zhao, C.Y. Su, Y.X. Tong, Porous Pt-Ni-P composite nanotube arrays: highly electroactive and durable catalysts for methanol electrooxidation. J. Am. Chem. Soc. **134**(13), 5730–5733 (2012). doi:10.1021/ja212206m

50. B. Habibi, E. Dadashpour, Carbon-ceramic supported bimetallic Pt-Ni nanoparticles as an electrocatalyst for electrooxidation of methanol and ethanol in acidic media. Int. J. Hydrog. Energy **38**(13), 5425–5434 (2013). doi:10.1016/j.ijhydene.2012.06.045